THE JOURNAL OF PHYSICAL CHEMISTRY C
A JOURNAL OF THE AMERICAN CHEMICAL SOCIETY

pubs.acs.org/JPCC

Article

Size Effects in Gold Nanorod Light-to-Heat Conversion under Femtosecond Illumination

Published as part of The Journal of Physical Chemistry virtual special issue "125 Years of The Journal of Physical Chemistry".

Sean M. Meyer, Jacob Pettine, David J. Nesbitt, and Catherine J. Murphy*

Cite This: *J. Phys. Chem. C* 2021, 125, 16268–16278

Read Online

ACCESS | Metrics & More | Article Recommendations | Supporting Information

ABSTRACT: The relative contributions of absorption vs scattering phenomena in plasmonic nanoparticles are pivotal to optimizing light-to-heat conversion efficiency, which is of particular interest in plasmonic photothermal therapy and targeted destruction of pathogenic cells, among other applications. The present study focuses on an explicit comparison of light-to-heat conversion efficiency in gold nanorods of identical aspect ratios but four different volumes, based on tunable ultrafast laser excitation, diffuse reflectance spectroscopy, and finite element simulations. Systematic analysis of photothermal properties under low-intensity femtosecond illumination reveals that larger-volume gold nanorods in colloidal solution have comparable performance to much smaller rods in overall photothermal conversion efficiency at identical optical density but behave quite differently from expectations based on diffuse reflectance spectroscopy. In addition, although the smallest rods exhibit equivalent photothermal conversion efficiencies to rods 10 times larger in volume, the temperature increase per rod is 4 times lower. These results show that the larger gold nanorods with high scattering still possess strong photothermal capabilities, which rival that of smaller rods on an ensemble level, and surpass small rods in both single-particle temperature increases and volume-normalized extinction.

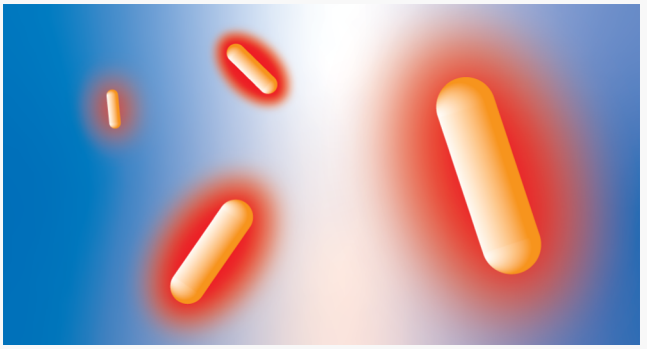

INTRODUCTION

Gold nanorods (AuNRs) are a class of plasmonic nanomaterials that interact strongly with light and possess sensitive size- and shape-dependent properties. Illumination at the resonant frequency induces a coherent oscillation of conduction-band electrons, known as a localized surface plasmon resonance (LSPR), which can decay either (i) radiatively via resonant scattering or (ii) nonradiatively into electron−hole excitations, which subsequently thermalize and induce lattice heating.[1−3] The resonant frequency of this plasmon oscillation can be tuned dramatically by altering either the nanorod aspect ratio (i.e., length-to-width ratio) or the volume of the nanoparticle. However, whether the plasmon decays radiatively or nonradiatively depends primarily on the volume of the particle, with little effect from the aspect ratio.[4,5]

Applications of AuNRs take advantage of the confined electric field at the particle surface and within the particle volume, along with the subsequent light scattering, charge currents, and/or heat generation.[6−12] Achieving a predictive understanding of how nanoparticles distribute incident optical energy has been a longstanding challenge, which has been difficult to address experimentally with a high degree of certainty.[13,14] It is well known that increasing the nanoparticle size increases the relative contributions of scattering (which scales quadratically with volume) vs absorption (which scales linearly with volume) to the total extinction cross-section.[15] As a result, smaller particles have been conventionally considered advantageous for targeted heating applications, since the extinction coefficient for such smaller AuNR species arises almost entirely from absorption.[13] Conversely, large scattering components of the extinction cross section are thought more suitable for bioimaging or other applications in which absorption losses are detrimental. In some cases, such as plasmon-enhanced spectroscopy/fluorescence, a sizeable contribution of both is desirable.[16,17] Thus, characterization of the absorption-to-extinction ratio is typically used to predict which size or shape particle is best for a system, particularly for

Received: April 30, 2021
Revised: July 3, 2021
Published: July 20, 2021

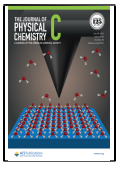

https://doi.org/10.1021/acs.jpcc.1c03898
J. Phys. Chem. C 2021, 125, 16268−16278

heating applications, as larger absorption-to-extinction ratios imply the more efficient conversion of light into heat.

However, knowledge of the absorption-to-extinction ratio by itself is often insufficient, as other ensemble contributions can also play a significant role in determining light−matter interactions. Indeed, while the absorption-to-extinction ratio is often calculated for a single particle and can be directly scaled up to predict ensemble properties,[18−20] the collective effects of many-particle heating in a solution can result in significant disagreement between measurement and predicted photothermal efficiency. For instance, Mackey et al. demonstrated that despite higher absorption-to-extinction ratios predicted from single-particle simulations for the smallest of three gold nanorod sizes, the weaker optical extinction per particle necessarily requires significantly larger particle concentrations to achieve the same photothermal effect, which is not ideal for cellular applications.[21] Additionally, multiple photon−particle interactions at these higher concentrations can effectively increase the path length for resonantly scattered photons, such that highly scattering particles can exhibit larger-than-predicted heating. This contributes to the loss of surface-enhanced Raman scattering intensity in colloidal solutions.[22,23] In addition, the use of intense laser light (whether in situ or in vivo) can cause photothermal reshaping, nanobubble formation, or modulation of the extinction cross section, all of which can lead to difficulty in accurately predicting the photothermal response.[24−28] These factors, along with a myriad experimental setups and assumptions, have led to inconsistent reports in the literature of photothermal efficiencies, even for the same particle type. A systematic study of the optical and corresponding photothermal properties of AuNRs with the same aspect ratio but the varying volume would therefore be valuable to better utilize and predict AuNR properties for a wide variety of applications.[29,30]

In this work, we first synthesize a series of AuNRs with different volumes but constant aspect ratios using well-established seed-mediated growth methods across the entire achievable size range of AuNRs from the literature.[31−33] The AuNRs are subsequently purified and characterized using transmission electron microscopy (TEM), ultraviolet−visible extinction spectroscopy (UV−vis), and diffuse reflectance spectroscopy. We utilize diffuse reflectance measurements with an integrating sphere in colloidal solution to determine absorption-to-extinction ratios and compare these values with theoretical finite element simulations. Such diffuse reflectance methods have been utilized previously to measure scattering from single particles on an immobilized slide under pulsed illumination, as well as silver nanoparticles and gold nanorod solution ensembles.[13,34−36] Colloidal solutions of AuNRs are then exposed to an ultrafast laser source tuned to the longitudinal LSPR for each particle, at three different power levels to measure their photothermal response under thermal steady-state conditions. These studies do reveal a systematic decrease in photothermal efficiency with increasing AuNR size, but much less so than expected from both calculation and diffuse reflectance spectroscopy measurement. Specifically, we find that the smallest rods convert the same fraction (within experimental uncertainty) of incident optical power into heat as rods 4-fold larger in volume. Indeed, at the same incident laser intensity, we observe only a 20% increase in photothermal heating for constant aspect ratio AuNRs with volumes varied over 2 orders of magnitude, which is unexpected given conventional scaling expectations.

EXPERIMENTAL METHODS

Materials. Gold(III) chloride trihydrate (>99.9% trace metals, 520918-25G), L-ascorbic acid (BioXtra >99%, A5960-25G), silver nitrate (ACS Reagent >99%, 209139-25G), concentrated HCl (37 wt %, 258148-4L), hydroquinone (H9003-500G, Reagent + grade), and cetyltrimethylammonium bromide (CTAB; for Molecular Bio >99%, H6269-1KG) are all purchased from Sigma-Aldrich. Sodium borohydride (AAS >99%, 71321-25G) is purchased from Fluka Analytical. 1 M HCl (1.0N, BDH7202-2) is purchased from VWR Chemicals. Sodium oleate (97% O005725G) is purchased from TCI America. Trisodium citrate dihydrate (>99%, S279-500) is purchased from Fisher Scientific. Thiolated monofunctional PEG (20k MW, PJK-602) is purchased from Creative PEGworks. Nanopure water is prepared using house deionized water in an 18.2 MΩ Barnstead II Nanopure System. All glassware and stir bars are rinsed with fresh aqua regia (3:1 concentrated HCl:HNO_3) and rinsed thoroughly with nanopure water.

Instrumentation. Electron micrographs are collected using a JEOL 2010 LaB_6 TEM operating at 200 kV, with over 100 particles measured using ImageJ. UV−vis extinction spectra are collected with an Agilent Cary 5000 UV−vis−NIR and absorption spectra are collected on an identical instrument equipped with an external DRA-1500 integrating sphere (Cary 2500 LabSphere, 150 mm diameter, ∼10% port fraction). A Mai-Tai HP Ti:Sapphire pulsed laser with 0.0113 cm^2 spot area, 100 fs pulse width, and an 80 MHz repetition rate was used in conjunction with a laser power meter and rotating linear polarizer for the laser-based measurements (Materials Research Lab UIUC).

Mini Rod Synthesis (Aspect Ratio = 3.6). The synthesis procedure for the mini nanorods has been described previously.[31] A 150 mL batch of AuNR is prepared based on this method. First, a ∼200 mL batch of small 1−2 nm gold seeds is prepared by adding 8.05 mL of ice-cold 0.01 M $NaBH_4$ to a quickly stirring solution (without excessive foaming of solution) of 200.85 mL 0.1 M CTAB and 5.15 mL 0.01 M $HAuCl_4{\cdot}3H_2O$. The solution turns a honey brown color. The seeds are stirred gently and aged for an hour before use. A growth solution is then prepared in a clean aqua regia rinsed 250 mL flask containing 150 mL 0.1 M CTAB, 10 mL 0.01 M $HAuCl_4{\cdot}3H_2O$, 1.5 mL of 0.01 M $AgNO_3$, 4 mL of 1 M HCl, 1.685 mL of 0.1 M ascorbic acid, and finally 50 mL of seed solution (added in that order). The contents are mixed well, covered with parafilm, and grown overnight for 16 h at room temperature. The next morning, the contents are split evenly between five 50 mL centrifuge tubes and centrifuged at 15500 rcf for 35 min. The colored supernatant is discarded, and the pellets are concentrated to 10 mL pure water in a new 15 mL centrifuge tube and centrifuged again at 14000 rcf for 35 min, with the final pellet dispersed into 5−10 mL of 1 mM CTAB.

Small Rod Synthesis (Aspect Ratio = 3.6). The synthesis of the small rods is performed using a previously described method.[32] First, a small batch of 1−2 nm gold seeds is prepared by adding 0.25 mL of 0.01 M $HAuCl_4{\cdot}3H_2O$ to 9.75 mL of 0.1 M CTAB and stirring as quickly as possible without foaming with a Teflon-coated stir bar. Then, 0.6 mL of ice-cold 10 mM $NaBH_4$ is quickly added to the stirring gold solution. The seeds turn a honey brown color and are aged for an hour before use. A growth solution is prepared in a 1 L aqua regia cleaned flask by adding 475 mL of 0.1 M CTAB, 25 mL

https://doi.org/10.1021/acs.jpcc.1c03898
J. Phys. Chem. C 2021, 125, 16268−16278

of 0.01 M $HAuCl_4 \cdot 3H_2O$, 4.25 mL of 0.01 M $AgNO_3$, 2.75 mL of 0.1 M ascorbic acid, and finally 0.6 mL of seed solution (in that order). The particles grow for at least 4 h and are then split equally among eleven 50 mL centrifuge tubes and centrifuged at 8000 rcf for 30 min, after which the pellets are combined in a fresh 15 mL tube with ∼10 mL water. The solution is again centrifuged at the same speed and dispersed into ∼5 mL 1 mM CTAB for long-term storage.

Medium Rod Synthesis (Aspect Ratio = 3.6). The synthesis method for the medium and large AuNRs is from Ye et al.[33] The first step, regardless of size, is the preparation of seeds, identical to the small rod procedure. Growth solutions are then prepared depending on the desired size. First, the smaller AuNR of width ∼32 nm is prepared as follows: 50 mL of 0.1 M CTAB is added to a 250 mL aqua-regia-cleaned flask equipped with a Teflon-coated stir bar and then heated to 50−60 °C while stirring gently, then 0.2470 g of sodium oleate is added and dissolved. After cooling to room temperature (∼28 °C), 4.8 mL of 4 mM $AgNO_3$ is added, and the solution sits for 10−15 min without stirring. We then begin stirring again and add 50 mL of 1 mM $HAuCl_4 \cdot 3H_2O$, stirred gently for 90 min. Then, 0.85 mL of 6 M HCl (prepared by diluting concentrated HCl 50%) is added and stirred gently for 10 more minutes. With stronger stirring, 250 μL of 64 mM ascorbic acid and shortly thereafter 20 μL of seed solution is added, with the resulting solution grown overnight for ∼16 h at room temperature. The particles are centrifuged at 1500 rcf for 30 min and dispersed into 10 mL of 1 mM CTAB, with a second repetition at 1200 rcf for 30 min, this time dispersing into 5 mL of 1 mM CTAB.

Large Rod Synthesis (Aspect Ratio = 3.6). For the largest AuNRs of the same aspect ratio (45 nm wide), an identical procedure to the medium rods is performed with only the following minor modifications: 1.2 mL of 6 M HCl and 2 μL of seeds are added, with the centrifuge speeds lowered to 1000 and 800 rcf for the first and second washes, respectively.

Medium and Large Rod Purification. Many spherical impurities are present in the final large rod samples, for which depletion-induced purification is performed to more cleanly isolate the desired AuNRs. The large dimensions of these rods make this a desirable method of purification.[37] Briefly, the ∼5 mL of raw particle solutions prepared in the synthesis are diluted down to 0.08−0.2 M total CTAB concentration by adding nanopure water and 0.2 M CTAB. The solution turns from a reddish-brown to a milky blue/purple color. The agglomerates can settle to the bottom overnight, leaving a pink solution behind (enriched in spheres). At this point, the supernatant is removed, with the process repeated until the UV−vis spectra of the supernatant reveal minimal spherical impurities. Different amounts of CTAB can be used to precipitate the rods from the solution, as it is dependent on the specific size; it is recommended to the interested reader to refer to the original paper for details on this method[41] and perform small additions of surfactant to see when agglomeration begins. For the large rods, this is around 0.08−0.1 M CTAB and for the medium rods around 0.15−0.2 M CTAB.

Photothermal Heating Experiment. The photothermal heating experiments are performed using a Mai-Tai HP Ti:Sapphire pulsed laser with a tunable wavelength from 690 to 1040 nm operating with 100−400 mW of average power, a pulse width of 100 fs, a repetition rate of 80 MHz, and a circular beam spot size area of 0.0113 cm^2, which translate into 1.25−5 nJ/pulse energies. A ∼2 mL Spectrosil fused silica cuvette equipped with a small Teflon-coated stir bar and thermocouple for temperature monitoring is placed on a small stir plate. Then, 2 mL of rod solution in 1 mM CTAB is added to the cuvette and set to gentle stirring on the center of the stir plate. The cuvette is stirred gently through the heating to ensure homogenous temperature change in the cell, as measured by a metal thermometer inserted through the top of the cuvette. A power meter (Thorlabs PM100D) is placed at the end of the stir plate in the beam path to monitor the laser power throughout the experiments. A rotatable polarizer is placed at the start of the beam path to smoothly adjust the transmitted beam power, with a digital thermometer next to the stirring plate to monitor the air temperature throughout the experiment. The solutions are then exposed to a systematic progression of laser power levels, heated to steady-state temperature conditions, and cooled naturally with stirring to determine the photothermal efficiency based on methods from the literature.[24,29,30] Using the temperature change with heat capacity of the cell, we can obtain the thermal heat power provided by the nanorods after illumination. This value is divided by the total extinct power measured from a power meter. For each rod type, at least three power levels are used to determine the photothermal efficiency, with the complete data acquisition for each power performed in triplicate. All rod solutions have the same optical density (OD = 1) at the excitation wavelength. Baseline contributions to heating are determined from known optical absorption coefficients at the incident wavelength, which are used to correct for heating of the neat (water) solvent. The heat dissipation term (τ) was measured by turning off the laser after initial excitation, measuring the temperature change for the subsequent 200 s, and fitting an exponential decay curve to this temperature change.

Integrating Sphere Measurements. Two separate Agilent Cary 5000 UV−vis spectrophotometers are used, one of which is equipped with a diffuse reflectance integrating sphere accessory (DRA-1500). The one without the integrating sphere (UV1) is used for all extinction measurements, and the one with the integrating sphere (UV2) is used for all of the absorption measurements. The spectra are scanned from 400 to 1100 nm at 0.1 s integration time, with a reduced slit height in UV2 measurements. In both instances, a 1 cm path length quartz cuvette is used, with a 2 mL rectangular quartz cuvette and 3 mL cylindrical quartz cuvette with a Teflon cap used for UV1 and UV2, respectively. Five milliliter solutions of different optical densities (OD 0.95−1.05 for small rods and OD 0.2−0.4 for the large rods) are prepared and their extinction are measured using UV1. The particles are then taken to UV2, placed at an angle of 25° normal to the incident light, and measured for their absorbance. The maximum values at the LSPR from UV1 and UV2 are used to determine the optical scattering/absorbance percentage of total extinction by dividing the extinction value from UV1 by the absorption value from UV2.

Determination of Extinction Coefficients. Reliable sources exist in the literature for single-rod extinction coefficients for small rods and mini rods,[31,38] but to the best of our knowledge, there are no experimentally determined extinction coefficients for rods similar in size to the medium and large rods. To determine these values, inductively coupled plasma mass spectrometry (ICP-MS) is used (University of South Carolina Mass Spectrometry Facility). A solution of particles in water with a known optical extinction is wholly

https://doi.org/10.1021/acs.jpcc.1c03898
J. Phys. Chem. C 2021, 125, 16268−16278

digested and atomic gold content is analyzed. Then, by correlation with TEM, at least 300 AuNRs were measured for their length and width and assumed to be a hemispherical tipped cylinder. This, along with the density of gold, was used to calculate the average volume of the AuNRs. Then, based on this information, the concentration of individual particles in the known extinction solution is determined, with the error bars arising from heterogeneity in the volume/size of the AuNRs.

Simulation Parameters. Electromagnetic finite element simulations are performed in the frequency domain with the RF module in COMSOL Multiphysics 5.4. All AuNRs are modeled as right cylinders with hemispherical endcaps, using the complex dielectric function measured for bulk gold.[39] Dimensions are based on statistical TEM characterization of the different samples. Ligand effects are neglected, and the background medium is taken to be pure water (real refractive index of 1.33). Under these conditions, absorption, scattering, and total extinction cross-sections are each calculated via multiple methods (Supporting Information Section 1). All methods agree to within a few percent. Further due diligence is performed by refining the mesh and adjusting the domain to ensure convergence and minimization of numerical artifacts.

RESULTS

The rigorous comparison of photothermal efficiency measurements for different absolute sizes of the same plasmonic nanomaterials requires the synthesis of, in our case, AuNRs of tunable absolute dimensions and we provide the dimensions of all rods in Table 1. We note that while our nomenclature of "mini, small, medium, large" is not standard in the literature, these rods encompass the most common achievable size range of AuNRs using seed-mediated methods. The mini, small, medium, and large rods, all of which are aspect ratio 3.6 (see the Experimental Methods section), have volumes of 1750 ± 740, 8700 ± 2480, 89400 ± 13700, and 256000 ± 37500 nm^3, respectively, where the error is the standard deviation from the TEM measurements. The physical and optical data are summarized in Figure 1 and Table 1. While the aspect ratio is held constant, plasmonic frequencies shift to lower energies with increasing size due to retardation effects.[40] There is also a coincident increase in plasmon width as the size increases, which is expected from the radiative damping in larger particles (Figure 1A).[41,42] The mini rods are an exception to this rule with the broadest plasmon width, which is attributed to the high polydispersity of the sample. The wavelengths associated with the different nanorod sample longitudinal plasmon resonances are 768, 783, 842, and 873 nm in 1 mM CTAB solution. To estimate their concentration in solution, molar extinction coefficients of the rods are required. While literature references exist for mini[31] and small[38] rods, the extinction coefficients for the medium and large rods are determined via ICP-MS correlated with UV−vis, as described in the Experimental Methods section. From these results and from the literature, the molar extinction coefficients are (2.0 ± 1.0) × 10^8, (4.6 ± 0.6) × 10^9, (6.0 ± 0.9) × 10^{10}, and (1.2 ± 0.2) × 10^{11} M^{-1} cm^{-1} for mini, small, medium, and large AuNRs, respectively, on a per-particle basis. The errors associated with the coefficients are based on the standard deviation for the volume measurements.

Table 1. Physical Dimensions of the AuNRs, Characterized by TEM[a]

rod type	length (nm)	width (nm)	volume (nm^3)
mini	30.9 ± 6.6	8.7 ± 1.2	1750 ± 740
small	52.9 ± 5.9	15.1 ± 1.9	8700 ± 2480
medium	118.8 ± 9.0	32.4 ± 2.2	89400 ± 13700
large	159.9 ± 12.7	47.9 ± 5.4	256000 ± 37500

[a]All errors are standard deviations, based on the measurement of over 100 AuNRs of each type.

Following the synthesis and characterization of the AuNRs, a theoretical simulation was used to compare against the real AuNRs as well as calculate their extinction efficiency. We utilize finite element simulations to calculate the optical properties of nanoparticles in water, interacting with light polarized along their longitudinal axis (see the Experimental Methods section). The results from these calculations yield plasmonic maxima that are in good agreement with the measured values, as summarized in Table 2. The ratios of the absorption efficiencies to the total extinction efficiencies are determined by eq 1

$$\% \text{ absorption} = \frac{Q_{abs}}{Q_{ext}} \times 100\% \quad (1)$$

where Q_{abs} is the calculated absorption efficiency and Q_{ext} is the calculated extinction efficiency. As can be seen in Table 2 and Figure 2, the absorption contribution decreases (and the scattering contribution correspondingly increases) dramatically with size. The theoretical extinction efficiency (Q_{ext}; the ratio of the extinction cross section to the 2D areal projection of the nanorod) peaks for the medium rods and drops off for larger rods. This is an important observation, as the extinction efficiency dictates how strongly light can interact with the gold nanorods on a per-rod basis[4,5] and is expected to be weakest for the smallest particles and strongest for the largest. However, a discrepancy from this expected trend is observed: the mini rods have a smaller extinction efficiency than the small rods, which is unexpected and will be expanded upon further in the Discussion section.

To investigate the absorption percentage under precise optical conditions by directly measuring the scattered photons, a low-intensity white light experiment is performed with an integrating sphere mounted onto a UV−vis spectrometer. This experimental design has been shown to be useful for determining the relative contributions of either scattering or absorption to the total extinction for moderately sized AuNRs and silver nanoparticles.[13,34] However, errors at lower wavelengths (<680 nm) appear, which we suggest are the result of reabsorbed scattered light during the measurement. The integrating sphere works by distributing the transmitted and scattered light intensity from the sample uniformly over the sphere surface by a highly reflective sphere surface coating. The integration process is the result of many uniform scattering events on the sphere surface to effectively measure the light from all angles from the sample. However, if the sample can reabsorb this light to a considerable degree, then an artificially high absorption value will occur.[43,44] This is prevalent in all samples because, above the longitudinal plasmon frequency, the extinction is mainly due to absorption. If the sample is highly scattering, then this error would be alleviated. To avoid issues with this phenomenon, known plasmonic absorption and scattering standards are used to verify this technique's accuracy at the plasmonic maximum

https://doi.org/10.1021/acs.jpcc.1c03898
J. Phys. Chem. C 2021, 125, 16268−16278

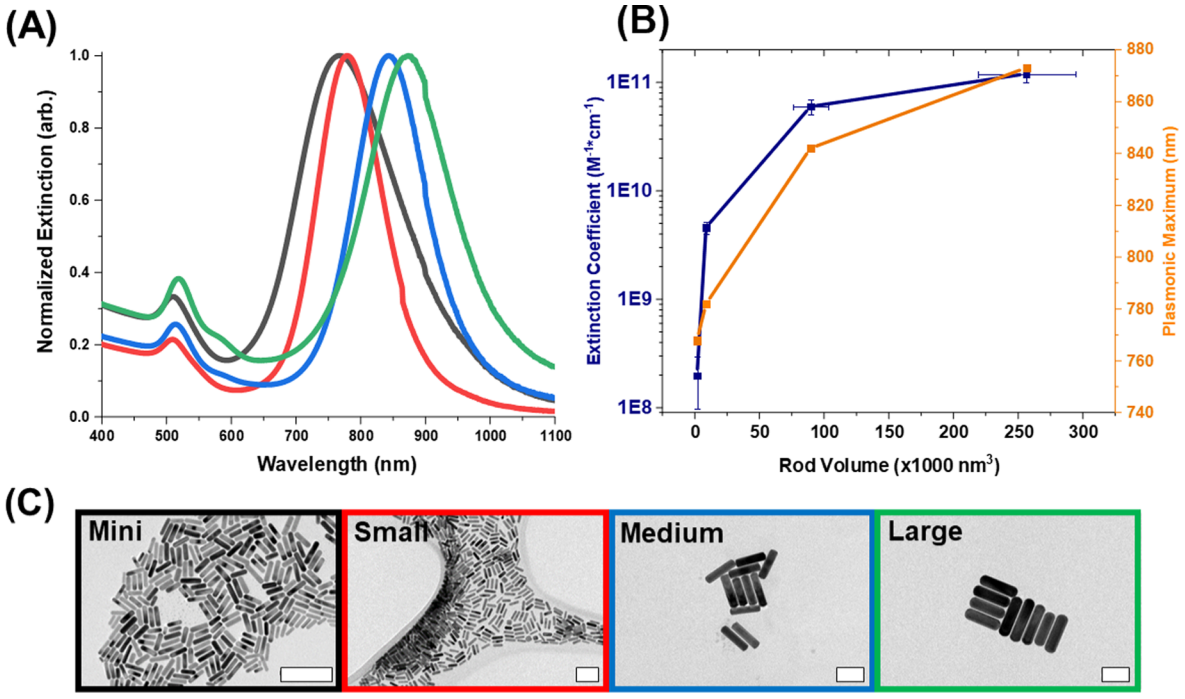

Figure 1. Complete optical and physical characterization of CTAB-coated AuNRs in water. (A) Representative normalized UV−vis extinction spectra for each rod type: mini (black), small (red), medium (blue), and large (green). (B) Extinction coefficients determined via ICP-MS and from the literature and measured plasmonic maxima vs particle volume. All rods share a similar aspect ratio of ∼3.6. (C) TEM micrographs of all nanorod samples (scale bars: 100 nm).

Table 2. Optical Characterization of the Gold Nanorods Used in This Study[a]

	LSPR (nm)		% absorption		
rod type	theory	exp.	theory	exp.	theoretical extinction efficiency σ_{ext}/A_{rod}
mini	754	772	98	96	19
small	761	780	89	91	30
medium	848	842	46	41	39
large	886	872	23	20	30

[a]The experimental absorption percentage of the total extinction inferred from the two measurements (diffuse reflectance and UV−vis extinction) at the longitudinal maximum using eq 1. The theoretical absorption percentage is derived from calculations using the finite element method. The theoretical extinction efficiency is the per-particle ratio of the optical-to-physical cross section calculated from the finite element method.

(Supporting Information, Section 2). In previous reports, this error is alleviated by normalizing the extinction and absorption spectra at 400 nm, assuming them to be identical at this wavelength.[13,54] As shown in Supporting Information, Section 2, the error is wavelength dependent; therefore, this approach will lead to incorrect results at the LSPR wavelength. The measurements at three different optical densities per rod type are performed and their results are averaged to obtain final absorption contributions to extinction for the mini, small, medium, and large rods of 96.4 ± 2.1, 91.2 ± 1.8, 41.3 ± 1.4, and 19.8 ± 0.8%, respectively, at the plasmonic maxima (errors are standard deviations of the mean from three measurements). The representative spectra obtained for each rod type are displayed in Figure 2A,B.

Following the characterization of the AuNR optical and physical properties, photothermal properties were measured. The photothermal efficiency η of an AuNR solution ensemble is defined as

$$\eta = \frac{P_{abs}}{P_0(1 - 10^{-OD})} \quad (2)$$

where P_{abs} is the power absorbed and converted to heat by AuNR ensembles (as determined by the temperature change of the solution and its total heat capacity), P_0 is the total input power to the cell before any extinction effects (as measured by the laser power meter), and OD is the optical density of the solution, accounting for both scattering and absorption contributions to the extinction. A heat transfer model is used to determine the heating efficiency based on the temperature rise for each rod type with the wavelength of the laser tuned to the plasmonic maximum[24,29]

$$C_{cell}\frac{\Delta T_{cell}}{\tau} = P_{base} + P_0(1 - 10^{-OD})\eta \quad (3)$$

in which C_{cell} is the total heat capacity of the cell (including the quartz cuvette and the solution), ΔT_{cell} is the temperature change of the cell with respect to its ambient temperature, τ = 408 ± 22 s is the thermalization time constant for the cell, and P_{base} is the baseline heat power input via the absorption of water. The total heat capacity is 8.37 J/K if just the solution is considered and approximately 15.8 J/K if the cuvette's entire mass is accounted for. A value of 14.5 J/K is used here to account for only the fraction of the quartz cuvette in contact with the heated solution (Supporting Information, Section 3). It is important to note that the photothermal efficiency determined via the heating of a particle solution is readily altered by assuming a different heat capacity for the cell. Therefore, the absolute values are not as reliable as the relative changes measured between the different rod types. The relative

https://doi.org/10.1021/acs.jpcc.1c03898
J. Phys. Chem. C 2021, 125, 16268−16278

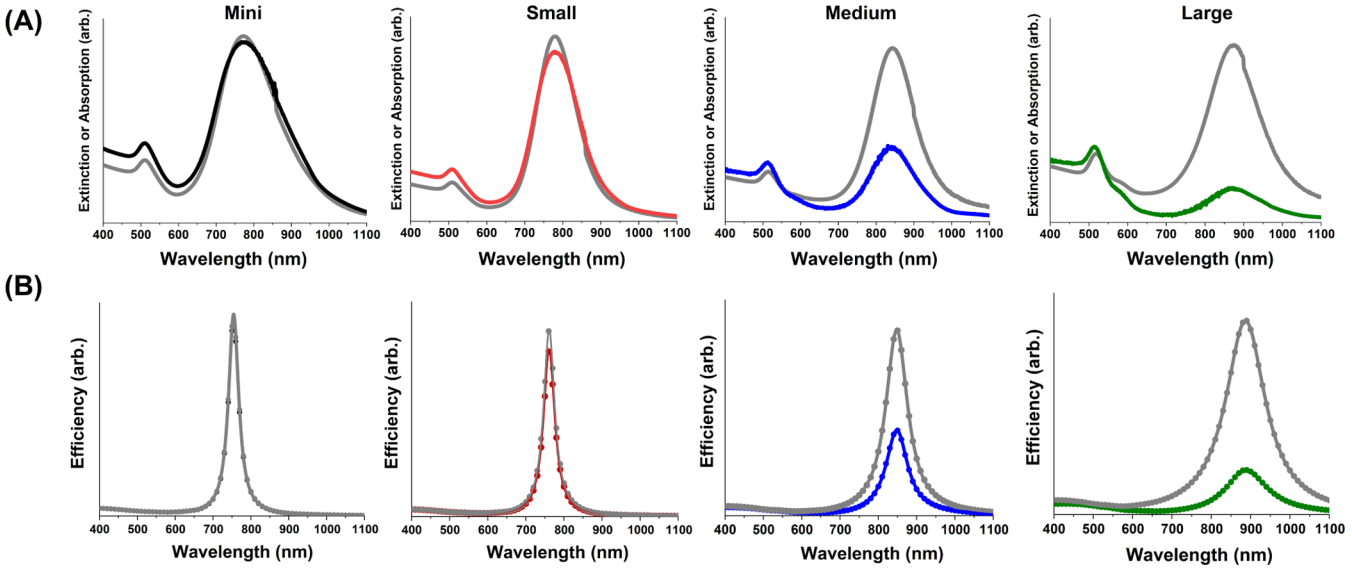

Figure 2. Comparison between measured and simulated extinction spectra. (A) Experimental diffuse reflectance spectra from the integrating sphere measurement (colored) and UV−vis extinction spectra (gray) for the four nanorod types in an aqueous solution. (B) Theoretical absorption (colored dots, with Lorentzian fits) and extinction (gray dots, with Lorentzian fits) efficiencies, calculated for single AuNRs.

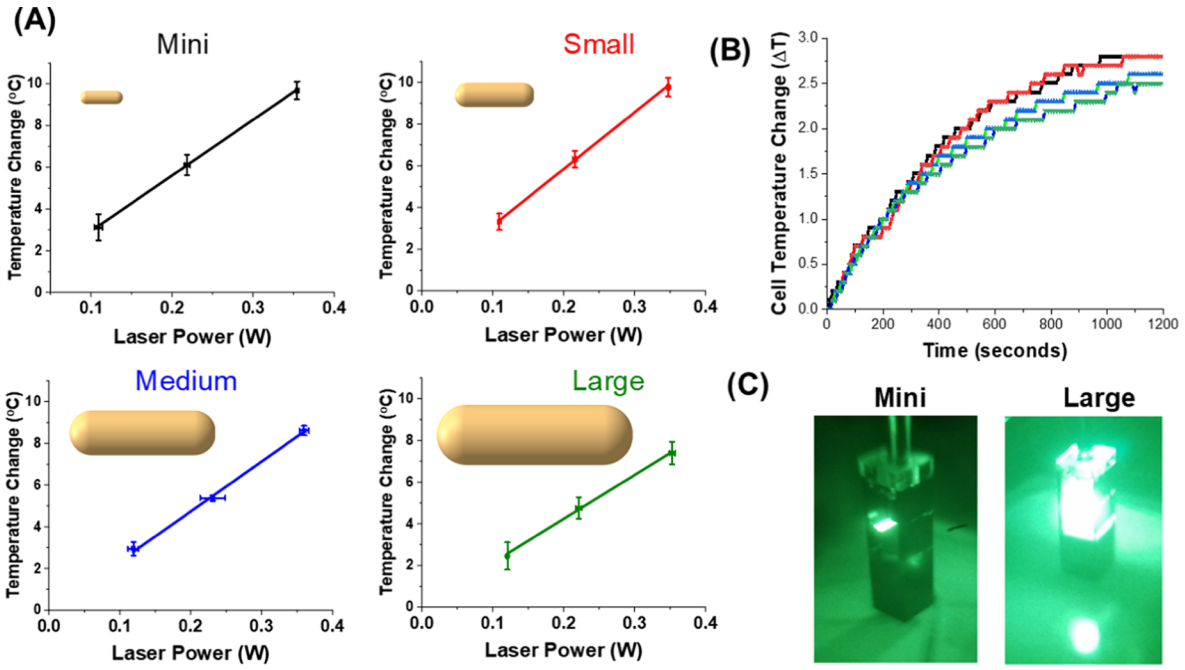

Figure 3. Photothermal behavior of colloidal solutions of gold nanorods of different absolute dimensions. (A) Equilibrium temperature change of the cell under illumination with varying laser powers. The slope of these lines is used to calculate photothermal efficiencies. (B) Representative cell temperature change over 1200 s to reach equilibrium for rods at a similar laser power (∼100 mW) for mini (black), small (red), medium (blue), and large rods (green). (C) Visual comparison of the large versus mini rod scattering intensities observed through an IR camera.

changes between the AuNRs are the critical feature, regardless of which heat capacity value is used. Indeed, this heat capacity variability likely represents a major contribution to the inconsistencies noted in the literature.

The laser system is tuned to the maximum LSPR extinction wavelength for each AuNR sample. The power extinction by the AuNRs vs the average temperature change is plotted in Figure 3A and fit to eq 3. The photothermal efficiency values for mini, small, medium, and large AuNRs are 103 ± 2, 105 ± 2, 87 ± 5, and 77 ± 4% (errors are standard deviations of the mean determined via three measurements). Values over 100% are attributed to an error in the approximate heat capacity, described above. The equilibrium temperature increase of the cell at different input powers is shown in Figure 3A for each rod size. These values follow the expectation that the photothermal efficiency will decrease with increasing volume, due to an increasingly large scattering contribution to the extinction. Figure 3B shows the representative temperature change of the cell over time for each rod type; the systems take approximately 1200 s to equilibrate. Additionally, in Figure 3C, the much more intense scattering due to the largest vs smallest

https://doi.org/10.1021/acs.jpcc.1c03898
J. Phys. Chem. C 2021, 125, 16268−16278

nanorods is clearly visible with an IR camera. The temperature rises are summarized in Supporting Information, Section 4.

The ensemble photothermal conversion efficiency determined above is a measure of the average heat power produced by the AuNR ensembles but does not provide any direct information on the individual temperature increase of each particle. This is difficult to achieve using continuous wave (CW) lasers because precise knowledge of the interfacial thermal conductivity is required to predict the equilibrium temperature rise of the particle under illumination.[25,28] By contrast, the temperature rise of each particle is readily estimated for femtosecond laser illumination, where the heating of the lattice on ~10 ps timescales is much faster than the heat is transferred to the surroundings on >100 ps timescales.[45,46]

The single-particle temperature increases after a single pulse, based on the number of rods in the solution and the average photothermal energy per rod, is given by eq 4, before heat dissipation to the surroundings[25]

$$\Delta T_{\mathrm{rod}} = \frac{P_0(1 - 10^{-\mathrm{OD}})\eta}{f_{\mathrm{rep}} Sl[\mathrm{Au}]c_{\mathrm{Au}}} \tag{4}$$

Here, ΔT_{rod} is the calculated temperature change of a single AuNR after a single femtosecond pulse, OD is the optical density at the LSPR wavelength, f_{rep} is the laser repetition rate, l is the path length of the laser, [Au] is the mass concentration of the gold, c_{Au} is the specific heat capacity of gold, and S is the spot size of the laser pulse. The calculation for the [Au] is explained Supporting Information, Section 5. The curves in Figure 4 indicate a tradeoff: as size decreases, ΔT_{rod} also

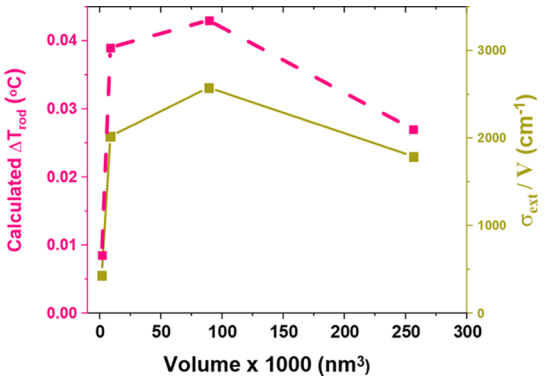

Figure 4. Calculated average temperature change of individual AuNRs of differing absolute dimensions following a 100 fs pulse. The temperature change of a single rod theoretically is determined (dashed pink) using eq 4. The gold line is the volume-normalized extinction cross section using eq 5.

decreases despite the increased photothermal efficiency. Using experimentally determined molar extinction coefficients, volume-normalized extinction cross-sections are given by[5,13,47]

$$\frac{\sigma_{\mathrm{ext}}}{V} = \frac{1000 \ln(10)\, \epsilon_{\mathrm{ext}}}{N_{\mathrm{A}} V} \tag{5}$$

where N_{A} is Avogadro's number (Supporting Information, Section 6). The volume-normalized extinction cross-section provides an effective means of comparing optical properties between different volume AuNRs and clarifies the drop in heating for the mini rods observed in Figure 4.[5]

DISCUSSION

A variety of gold nanoparticle applications rely on their ability to convert light into heat, with size having the most important influence on photothermal properties.[2,48] Many reports attempting to answer the perennial question of "Which particle size is best for my system?" have been released in the past two decades. Figure 5 compares various reports from the literature,

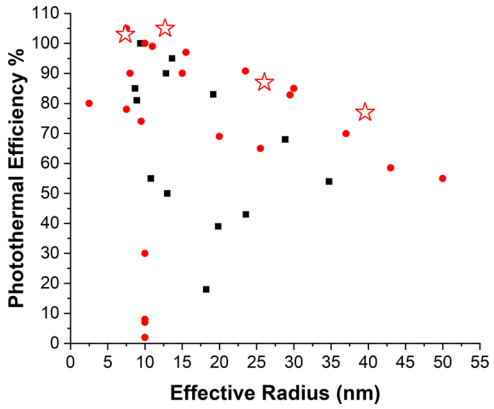

Figure 5. Summary of literature values of photothermal efficiency (eq 2) for gold nanoparticles. The black squares represent AuNRs, the red circles represent Au spheres, and the red stars are the results from this study. The corresponding references are summarized in Supporting Information, Section 7. Average values only are reported, with no error bars, for clarity.

showing wide disagreement; there is a general trend of increasing size producing lower photothermal efficiency, but there are many outliers, and it is thus difficult to discern which particle type has the "best" performance.[18−20,24,49−55] For instance, Roper et al.[19] and Qin et al.[20] both measure the heating of a solution of small Au spheres with a CW laser near the plasmon resonance but find differences in photothermal efficiency of nearly 90%. Roper et al. utilize a small droplet of particles, whereas Qin et al. measure a stirring cuvette filled with particle solution. Similarly, Cole et al.[24] find a photothermal efficiency of 60% for 44 nm × 13 nm AuNRs, while Qin et al. find 100% for similar particles. In the works summarized in Figure 5, different setups (cuvette vs droplet), wavelengths of excitation not centralized at the LSPR, and the neglect of ensemble effects all lead to discrepancies in reported photothermal efficiencies, even for similar particles. Additionally, measuring photothermal efficiencies via the temperature change of a solution is problematic, involving assumptions/approximations of the heat capacity of the surrounding environment/cell.[56] In the present work, investigations of the extinction of each rod type not only with photothermal heating but also measurement of absorption vs extinction via diffuse reflectance with an integrating sphere provide clarifying data.

The most discussed parameter in the nano-plasmonic thermal energy conversion literature is the overall photothermal efficiency of nanoparticle ensembles (eq 2), but rarely are single-particle performances addressed. Both pulsed and CW lasers have been used for photothermal applications; both have advantages and disadvantages.[30,57] The peak pulse powers used herein remain well below the threshold for heat-induced particle deformation, as verified in Supporting Information, Section 8.[58] Resonant femtosecond pulsed excitation can be described in three steps:[1,3] First, plasmon oscillations decay into electron−hole excitations, which thermalize within several

https://doi.org/10.1021/acs.jpcc.1c03898
J. Phys. Chem. C 2021, 125, 16268−16278

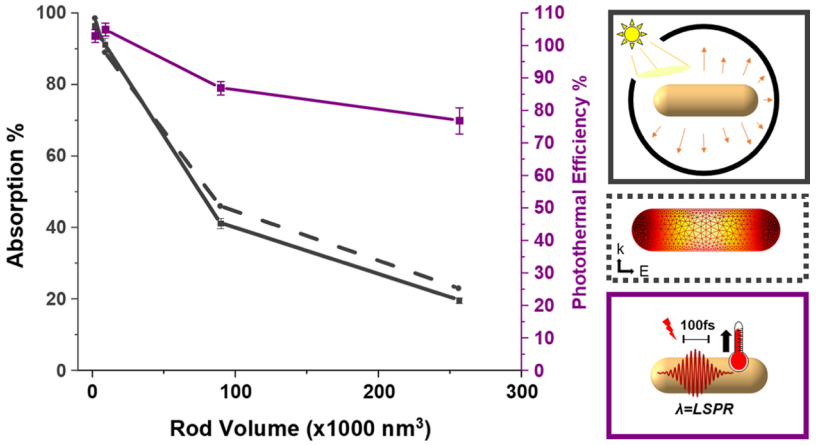

Figure 6. Summary of each absorption characterization method plotted vs AuNR volume. The percent absorption is plotted for diffuse reflectance measurements (solid gray) and finite element simulations (dashed gray), whereas the photothermal efficiency is plotted for the photothermal data (solid purple).

hundred femtoseconds via electron−electron scattering. The hot electrons then transfer energy to the gold lattice within a few picoseconds via electron−phonon scattering throughout the particle. Finally, the particle transfers this heat to the surroundings after hundreds of picoseconds to a few nanoseconds. Typically, even for largest nanoparticles, the system will equilibrate with the environment within a few nanoseconds.[25,26] For femtosecond laser pulses, it has been theoretically shown that the light excitation and particle heating are separated in time, except for the case of extremely small particles (<5 nm dimensions). This separation of timescales allows for the reliable estimation of the average particle temperature rise following excitation by a femtosecond pulse.[45,46,59]

The results of the photothermal measurements shown in Figure 6 exhibit the expected behavior, i.e., increasing the particle volume while maintaining the same optical density will lower the photothermal efficiency. The experimental diffuse reflectance and theoretical finite element methods agree with one another. However, as can be seen from Figure 6, photothermal efficiency percentages are far higher than expected for the larger rods based on the relative absorption. In examples from the literature (Figure 5), this is a common occurrence for particles that have large scattering cross sections relative to their absorption cross sections. One explanation for this phenomenon is that scattered photons can be reabsorbed by other nanorods in the colloidal solution; the larger scattering cross-sections for larger particles dramatically increase the likelihood of photons scattering multiple times in solutions. This can enhance absorption conversion significantly, as observed by Chen et al.[29] and Cole et al.[24] for gold bipyramids and nanoshells, respectively. This same phenomenon was found by Breghnoi et al.[60] to explain why larger gold nanorods exhibit stronger singlet oxygen generation. They deduced a linear relationship between the scattering efficiency of the particles and their ability to generate singlet oxygen. Additionally, An et al.[61] investigated the heating of a large cylinder of a solution of two sizes of gold nanorods under laser illumination. They found that for larger AuNRs, the solution becomes much hotter further away from the laser illumination zone than for the smaller rods, with the implication that heating larger particles yields more of a collective effect across the cell, resulting from the multiple light scattering. For our setup, like many others, the efficiency is determined by exposing a laser beam with a small spot size and high intensity. This may explain why there is no significant difference between the diffuse reflectance measurements and finite element simulations, as the spot size of the UV−vis is on the order of the size of the cuvette. Kuttner et al.[54] implemented a similar integrating sphere method to check the absorption-to-extinction ratio of AuNRs coated with Au nanospheres and exposed the cuvette to a laser with a spot size equivalent to the cuvette window. They found that the measured efficiency was very close to the theoretically determined absorption to extinction ratio. The implications of these results are that while temperature measurements are reasonable to compare the photothermal efficacy of various AuNRs, the integrating sphere measurement aligns more closely to theory and provides an absolute measurement of absorption and scattering.

Comparing the photothermal conversion efficiencies of the rods in Figure 6, it is clear there that there is only a minor difference between the mini and small rods. It should also be noted that even the large rods, though significantly more voluminous than mini rods, still have high (>70%) photothermal efficiency. In other words, increasing the gold nanorod volume by nearly 150× (from mini to large rods) only decreases the photothermal efficiency by 20%, instead of a theoretical prediction of 80% based on the measured absorption-to-extinction ratio. As mentioned previously, caution must be exercised in measurements of absolute photothermal efficiencies, as the literature values change dramatically between nominally identical nanoparticle systems (Figure 5 and Supporting Information, Section 7) due to differences in experimental setup and ensemble effects. Interestingly, for the largest rods, diluting the rods 20-fold produced a photothermal efficiency of 69 ± 6%, which is statistically identical to that of the original solution of large rods. The large rods maintain their increased photothermal efficiency which could be a result of the maintained multiple scattering effects even at low concentrations.[22,61,62] Using the theoretical absorption over extinction ratios and the experimental extinction coefficients, we can calculate that the large rods have an absorption coefficient over 2 orders of magnitude greater than the mini rods. This consideration implies that the large particles still have large absorption cross sections, even

https://doi.org/10.1021/acs.jpcc.1c03898
J. Phys. Chem. C 2021, 125, 16268−16278

with high scattering efficiencies which promote intense heating at low concentrations.[64]

For a more in-depth look at the particle heating process, the temperature change following a single pulse can be used to estimate how hot the illuminated region becomes after femtosecond illumination and can be modeled theoretically (eq 4).[45,46,62−64] The mini rods do not collectively become as hot as the small rods after a single pulse, likely because their extinction efficiency and volume-normalized extinction cross section are low compared to the other particles. Interestingly, there is a drop-off in the temperature rise of the large rods, despite a large increase in volume, which is reflected in the volume-normalized extinction cross section and theoretical cross-section calculations. In Figure 4, the volume-normalized extinction cross sections vs volume reveal that the mini rods have a volume-normalized extinction cross section 4-fold smaller than the small rods, which implies that their small size limits their efficiency as optical transducers, and that a size increase is generally beneficial.[5] Using the extinction coefficients for each rod type, the gold mass concentration for the mini, small, medium, and large rods was 0.102, 0.0220, 0.0174, and 0.0248 g/L, respectively, at OD = 1. Therefore, the mini rods require significantly more gold to produce a similar optical effect as the other gold nanorods, for example, the medium rods produce close to 90% of the heat at identical OD while utilizing only 17% of the gold as the mini rods. This same effect is true even for CW illumination because the particle temperature change under CW illumination is proportional to $\sigma_{ext}\ \eta/R_{eff}$, where R_{eff} is the radius of a sphere with equivalent volume to the nanoparticle.[56]

These results demonstrate that smaller may not always be better for heating applications, as ensemble effects (such as multiply scattered photons) of the larger rods can lead to strong photothermal conversion efficiencies giving them hotter-than-expected responses. Even at the single-particle level, larger rods can become significantly hotter (see, e.g., Figure 4) and may therefore be preferred for some plasmonic photothermal applications. Additionally, the diffuse reflectance measurements and individual particle temperature rise analyses indicate that photothermal efficiency measurements are not a highly reliable means of comparing different particles, as even the large relative increase in the scattering cross-sections of larger particles does not lower the photothermal efficiency of the ensemble as drastically as expected from simple absorption-to-extinction ratio considerations. Photothermal therapies require that particles penetrate and localize in a cellular region with high enough concentrations to induce cell death under photothermal heating.[21,64] Under pulsed illumination, the temperature jump is highly localized to the particle and its immediate surroundings following excitation and maximizing this temperature rise is important for the efficacy of photothermal therapies.[62] Hence, larger particles may be more useful for this type of system. For CW illumination, where the goal is often to heat a macroscale volume to a higher temperature, mini rods might still be preferable because of their higher penetration into cells and enhanced loading over larger rods.[11,19,64] In addition to a comparison of nanoparticle performance, the results herein suggest that a combination of absolute scattering/absorption measurements and theoretical analyses should be utilized to understand the fundamental properties of plasmonic nanoparticles.

CONCLUSIONS

We have studied the dependence of AuNR light-to-heat conversion and optical properties as a function of rod volume for a constant aspect ratio. The entire range of readily accessible rod sizes (based on the most common synthetic methods in the literature) has been investigated using photothermal, diffuse reflectance, and theoretical methods. The smallest gold nanorods, while theoretically exhibiting the highest absorption/extinction ratio, suffer from poor optical absorption efficiency; slightly larger rods are therefore advantageous due to their high absorption efficiency and ability to produce similar amounts of heat at much lower gold concentrations. Large, highly scattering nanorods exhibit higher-than-expected photothermal efficiency and have large per-particle temperature increases resulting from multiple scattering effects and large absorption cross sections. Interestingly the smallest particles reach a fraction of the temperature increase as larger particles of nearly the same absorption to extinction ratio at the single-particle level. These results imply that "large" gold nanorods are potentially beneficial for photothermal activity over the smallest possible rods depending on the desired application.

ASSOCIATED CONTENT

Supporting Information

The Supporting Information is available free of charge at https://pubs.acs.org/doi/10.1021/acs.jpcc.1c03898.

List of equations and variables used to calculate the optical components of the AuNRs using FEM simulations; analysis of integrating sphere measurement integrity using highly absorptive and highly scattering samples; calculation to determine how much of the cuvette to include in the heat capacity of the cell; total summary of heating values obtained from different laser powers and different AuNRs; calculation of [Au] (g/mL) for each solution of AuNRs; derivation of the volume-normalized extinction cross section for each type of AuNR; complete summary of references included in Figure 1, along with particle dimensions and a description of all photothermal setups; confirmation of the structural integrity of the AuNRs following pulsed illumination (PDF)

AUTHOR INFORMATION

Corresponding Author

Catherine J. Murphy − *Department of Chemistry, University of Illinois at Urbana-Champaign, Urbana, Illinois 61801, United States;* orcid.org/0000-0001-7066-5575; Email: murphycj@illinois.edu

Authors

Sean M. Meyer − *Department of Chemistry, University of Illinois at Urbana-Champaign, Urbana, Illinois 61801, United States;* orcid.org/0000-0003-0771-5095

Jacob Pettine − *JILA, University of Colorado Boulder and National Institute of Standards and Technology, Boulder, Colorado 80309, United States; Department of Physics, University of Colorado Boulder, Boulder, Colorado 80309, United States;* orcid.org/0000-0003-2102-1743

David J. Nesbitt − *JILA, University of Colorado Boulder and National Institute of Standards and Technology, Boulder, Colorado 80309, United States; Department of Chemistry*

and Biochemistry and Department of Physics, University of Colorado Boulder, Boulder, Colorado 80309, United States; orcid.org/0000-0001-5365-1120

Complete contact information is available at: https://pubs.acs.org/10.1021/acs.jpcc.1c03898

Notes

The authors declare no competing financial interest.

■ ACKNOWLEDGMENTS

This research was carried out in part in the Materials Research Laboratory Central Research Facilities, University of Illinois. The authors thank Dr. Jordan Dennison for help in the initial stages with setting up the experiments, Dr. Prashant Jain for providing constructive feedback during the writing process, and Dr. Julio Soares for help with setting up and troubleshooting the laser setup. This work has been supported by the Air Force Office of Scientific Research (FA9550-15-1-0090) with additional funds for laser and apparatus development provided by the National Science Foundation Physics Frontier Center (PHY-1734006), and by the National Science Foundation (CHE-1608743).

■ REFERENCES

(1) Link, S.; El-Sayed, M. A. Shape and Size Dependence of Radiative, Non-Radiative and Photothermal Properties of Gold Nanocrystals. *Int. Rev. Phys. Chem.* **2000**, *19*, 409−453.
(2) Chen, H.; Shao, L.; Li, Q.; Wang, J. Gold Nanorods and Their Plasmonic Properties. *Chem. Soc. Rev.* **2013**, *42*, 2679−2724.
(3) Link, S.; El-Sayed, M. A. Spectral Properties and Relaxation Dynamics of Surface Plasmon Electronic Oscillations in Gold and Silver Nanodots and Nanorods. *J. Phys. Chem. B* **1999**, *103*, 8410−8426.
(4) Lee, K.-S.; El-Sayed, M. A. Dependence of the Enhanced Optical Scattering Efficiency Relative to That of Absorption for Gold Metal Nanorods on Aspect Ratio, Size, End-Cap Shape, and Medium Refractive Index. *J. Phys. Chem. B* **2005**, *109*, 20331−20338.
(5) Jain, P. K.; Lee, K. S.; El-Sayed, I. H.; El-Sayed, M. A. Calculated Absorption and Scattering Properties of Gold Nanoparticles of Different Size, Shape, and Composition: Applications in Biological Imaging and Biomedicine. *J. Phys. Chem. B* **2006**, *110*, 7238−7248.
(6) Norman, R. S.; Stone, J. W.; Gole, A.; Murphy, C. J.; Sabo-Attwood, T. L. Targeted Photothermal Lysis of the Pathogenic Bacteria, Pseudomonas Aeruginosa, with Gold Nanorods. *Nano Lett.* **2008**, *8*, 302−306.
(7) Wang, H.; Huff, T. B.; Zweifel, D. A.; He, W.; Low, P. S.; Wei, A.; Cheng, J.-X. In Vitro and In vivo Two-Photon Luminescence Imaging of Single Gold Nanorods. *Proc. Natl. Acad. Sci. USA* **2005**, *12*, 15752−15756.
(8) Reguera, J.; Langer, J.; Jimenez De Aberasturi, D.; Liz-Marzan, L. M. Anisotropic Metal Nanoparticles for Surface Enhanced Raman Scattering. *Chem. Soc. Rev.* **2017**, *46*, 3866−3885.
(9) Jokerst, J. V.; Thangaraj, M.; Kempen, P. J.; Sinclair, R.; Gambhir, S. S. Photoacoustic Imaging of Mesenchymal Stem Cells in Living Mice via Silica-Coated Gold Nanorods. *ACS Nano* **2012**, *6*, 5920−5930.
(10) Tian, L.; Chen, E.; Gandra, N.; Abbas, A.; Singamaneni, S. Gold Nanorods as Plasmonic Nanotransducers: Distance-Dependent Refractive Index Sensitivity. *Langmuir* **2012**, *28*, 17435−17442.
(11) Murphy, C. J.; Chang, H.-H.; Falagan-Lotsch, P.; Gole, M. T.; Hofmann, D. M.; Hoang, K. H. L.; McClain, S. M.; Meyer, S. M.; Turner, J. G.; Unnikrishnan, M.; et al. Virus-Sized Gold Nanorods: Plasmonic Particles for Biology. *Acc. Chem. Res.* **2019**, *52*, 2124−2135.
(12) Pettine, J.; Meyer, S. M.; Medeghini, F.; Murphy, C. J.; Nesbitt, D. J. Controlling the Spatial and Momentum Distributions of Plasmonic Carriers: Volume vs Surface Effects. *ACS Nano* **2021**, *15*, 1566−1578.
(13) Park, K.; Biswas, S.; Kanel, S.; Nepal, D.; Vaia, R. A. Engineering the Optical Properties of Gold Nanorods: Independent Tuning of Surface Plasmon Energy, Extinction Coefficient, and Scattering Cross Section. *J. Phys. Chem. C* **2014**, *118*, 5918−5926.
(14) Tcherniak, A.; Ha, J. W.; Dominguez-Medina, S.; Slaughter, L. S.; Link, S. Probing a Century Old Prediction One Plasmonic Particle at a Time. *Nano Lett.* **2010**, *10*, 1398−1404.
(15) Bohren, C. F.; Huffman, D. R. *Absorption and Scattering of Light by Small Particles*; Wiley, 1983.
(16) Ming, T.; Chen, H.; Jiang, R.; Li, Q.; Wang, J. Plasmon-Controlled Fluorescence: Beyond the Intensity Enhancement. *J. Phys. Chem. Lett.* **2012**, *3*, 191−202.
(17) Lin, K.-Q.; Yi, J.; Liu, B.-J.; Liu, J.-Y.; Wang, X.; Ren, B.; et al. Size Effect on SERS of Gold Nanorods Demonstrated via Single Nanoparticle Spectroscopy. *J. Phys. Chem. C* **2016**, *120*, 20806−20813.
(18) Richardson, H. H.; Carlson, M. T.; Tandler, P. J.; Hernandez, P.; Govorov, A. O. Experimental and Theoretical Studies of Light-to-Heat Conversion and Collective Heating Effects in Metal Nanoparticle Solutions. *Nano Lett.* **2009**, *9*, 1139−1146.
(19) Roper, D. K.; Ahn, W.; Hoepfner, M. Microscale Heat Transfer Transduced by Surface Plasmon Resonant Gold Nanoparticles. *J. Phys. Chem. C* **2007**, *111*, 3636−3641.
(20) Qin, Z.; Wang, Y.; Randrianalisoa, J.; Raeesi, V.; Chan, W. C. W.; Lipiński, W.; Bischof, J. C. Quantitative Comparison of Photothermal Heat Generation between Gold Nanospheres and Nanorods. *Sci. Rep.* **2016**, *6*, No. 29836.
(21) Mackey, M. A.; Ali, M. R. K.; Austin, L. A.; Near, R. D.; El-Sayed, M. A. The Most Effective Gold Nanorod Size for Plasmonic Photothermal Therapy: Theory and In Vitro Experiments. *J. Phys. Chem. B* **2014**, *118*, 1319−1326.
(22) Hogan, N. J.; Urban, A. S.; Ayala-Orozco, C.; Pimpinelli, A.; Nordlander, P.; Halas, N. J. Nanoparticles Heat through Light Localization. *Nano Lett.* **2014**, *14*, 4640−4645.
(23) Sivapalan, S. T.; DeVetter, B. M.; Yang, T. K.; van Dijk, T.; Schulmerich, M. V.; Carney, P. S.; Bhargava, R.; Murphy, C. J. Off-Resonance SERS from Gold Nanorod Suspensions as a Function of Aspect Ratio: Not What We Thought. *ACS Nano* **2013**, *7*, 2099−2105.
(24) Cole, J. R.; Mirin, N. A.; Knight, M. W.; Goodrich, G. P.; Halas, N. J. Photothermal Efficiencies of Nanoshells and Nanorods for Clinical Therapeutic Applications. *J. Phys. Chem. C* **2009**, *113*, 12090−12094.
(25) Nguyen, S. C.; Zhang, Q.; Manthiram, K.; Ye, X.; Lomont, J. P.; Harris, C. B.; Weller, H.; Alivisatos, A. P. Study of Heat Transfer Dynamics from Gold Nanorods to the Environment via Time-Resolved Infrared Spectroscopy. *ACS Nano* **2016**, *10*, 2144−2151.
(26) Hou, X.; Djellali, N.; Palpant, B. Absorption of Ultrashort Laser Pulses by Plasmonic Nanoparticles: Not Necessarily What You Might Think. *ACS Photonics* **2018**, *5*, 3856−3863.
(27) Lachaine, R.; Boulais, E.; Meuiner, M. From Thermo- to Plasma-mediated ultrafast laser-induced plasmonic nanobubbles. *ACS Photonics* **2014**, *1*, 331−336.
(28) Huang, J.; Park, J.; Wang, W.; Murphy, C. J.; Cahill, D. G. Ultrafast Thermal Analysis of Surface Functionalized Gold Nanorods in Aqueous Solution. *ACS Nano* **2013**, *7*, 589−597.
(29) Chen, H.; Shao, L.; Ming, T.; Sun, Z.; Zhao, C.; Yang, B.; Wang, J. Understanding the Photothermal Conversion Efficiency of Gold Nanocrystals. *Small* **2010**, *6*, 2272−2280.
(30) Abadeer, N. A.; Murphy, C. J. Recent Progress in Cancer Thermal Therapy Using Gold Nanoparticles. *J. Phys. Chem. C* **2016**, *120*, 4691−4716.
(31) Chang, H.-H.; Murphy, C. J. Mini Gold Nanorods with Tunable Plasmonic Peaks beyond 1000 nm. *Chem. Mater.* **2018**, *30*, 1427−1435.
(32) Sau, T. K.; Murphy, C. J. Seed High yield synthesis of short Au nanorods in aqueous solution. *Langmuir* **2004**, *20*, 6414−6420.

(33) Ye, X.; Zheng, C.; Chen, J.; Gao, Y.; Murray, C. B. Using Binary Surfactant Mixtures to Simultaneously Improve the Dimensional Tunability and Monodispersity in the Seeded Growth of Gold Nanorods. *Nano Lett.* **2013**, *13*, 765−771.
(34) Evanoff, D. D.; Chumanov, G. Size-Controlled Synthesis of Nanoparticles. 2. Measurement of Extinction, Scattering, and Absorption Cross Sections. *J. Phys. Chem. B* **2004**, *108*, 13957−13962.
(35) Olson, J.; Dominguez-Medina, S.; Hoggard, A.; Wang, L.-Y.; Chang, W.-S.; Link, S. Optical Characterization of Single Plasmonic Nanoparticles. *Chem. Soc. Rev.* **2015**, *44*, 40−57.
(36) He, G. S.; Zhu, J.; Yong, K.-T.; Baev, A.; Cai, H.-X.; Hu, R.; Cui, Y.; Zhang, X.-H.; Prasad, P. N. Scattering and Absorption Cross-Section Spectral Measurements of Gold Nanorods in Water. *J. Phys. Chem. C* **2010**, *114*, 2853−2860.
(37) Park, K.; Koerner, H.; Vaia, R. A. Depletion-Induced Shape and Size Selection of Gold Nanoparticles. *Nano Lett.* **2010**, *10*, 1433−1439.
(38) Orendorff, C. J.; Murphy, C. J. Quantitation of Metal Content in the Silver-Assisted Growth of Gold Nanorods. *J. Phys. Chem. B* **2006**, *110*, 3990−3994.
(39) Johnson, P. B.; Christy, R. W. Optical Constants of the Noble Metals. *Phys. Rev. B* **1972**, *6*, 4370−4379.
(40) Maier, S. A. *Plasmonics: Fundamentals and Applications*; Springer Science, 2007.
(41) Kelly, K. L.; Coronado, E.; Zhao, L. L.; Schatz, G. The Optical Properties of Metal Nanoparticles: The influence of Size, Shape, and Dielectric Environment. *J. Phys. Chem. B* **2003**, *107*, 668−677.
(42) Sönnichsen, C.; Franzal, T.; Wilk, T.; von Plessen, G.; Feldmann, J.; Wilson, O.; Mulvaney, P. Drastic Reduction of Plasmon Damping in Gold Nanorods. *Phys. Rev. Lett.* **2002**, *88*, No. 077402.
(43) Hodgkinson, J.; Masiyano, D.; Tatam, R. P. Using Integrating Spheres as Absorption Cells: Path-length Distribution and Application of Bee'rs Law. *Appl. Opt.* **2009**, *48*, 5748−5758.
(44) Gaigalas, A. K.; He, H.-J.; Wang, L. Measurement of Absorption and Scattering with an Integrating Sphere Detector: Application to Microalgae. *J. Res. Natl. Inst. Stand. Technol.* **2009**, *114*, 69−81.
(45) Baffou, G.; Rigneault, H. Femtosecond Pulsed Optical Heating of Gold Nanoparticles. *Phys. Rev. B* **2011**, *84*, 035415−035428.
(46) Ekici, O.; Harrison, R. K.; Durr, N. J.; Eversole, D. S.; Lee, M.; Ben-Yakar, A. Thermal Analysis of Gold Nanorods Heated with Femtosecond Laser Pulses. *J. Phys D: Appl. Phys.* **2008**, *41*, 185501−185512.
(47) Tang, J.; Gao, K.; Ou, Q.; Fu, X.; Man, S.-Q.; Guo, J.; Liu, Y. Calculation of Extinction Cross Sections and Molar Attenuation Coefficient of Small Gold Nanoparticles and Experimental Observation of Their UV−vis Spectral Properties. *Spectrochim. Acta, Part A* **2018**, *191*, 513−520.
(48) Burrows, N. D.; Lin, W.; Hinman, J. G.; Dennison, J. M.; Vartanian, A. M.; Abadeer, N. S.; Grzincic, E. M.; Jacob, L. M.; Li, J.; Murphy, C. J. Surface Chemistry of Gold Nanorods. *Langmuir* **2016**, *32*, 9905−9921.
(49) Jiang, K.; Smith, D. A.; Pinchuk, A. Size-Dependent Photothermal Conversion Efficiencies of Plasmonically Heated Gold Nanoparticles. *J. Phys. Chem. C* **2013**, *117*, 27073−27080.
(50) Liu, B.-J.; Lin, K.-Q.; Hu, S.; Wang, X.; Lei, Z.-C.; Lin, H.-X.; Ren, B. Extraction of Absorption and Scattering Contribution of Metallic Nanoparticles Toward Rational Synthesis and Application. *Anal. Chem.* **2015**, *87*, 1058−1065.
(51) Alrahili, M.; Peroor, R.; Savchuk, V.; McNear, K.; Pinchuk, A. Morphology Dependence in Photothermal Heating of Gold Nanomaterials with Near-IR Laser. *J. Phys. Chem. C.* **2020**, *124*, 4755−4763.
(52) Almada, M.; Leal-Martinez, B. H.; Hassan, N.; Kogan, M. J.; Buroba, M. G.; Topete, A.; Valdez, M. A.; Juarez, J. Photothermal Conversion Efficiency and Cytotoxic Effects of Gold Nanorods Stabilized with Chitosan, Alginate, and Poly(vinyl alcohol). *Mater. Sci. Eng. C* **2017**, *77*, 583−593.
(53) Chiu, M.-J.; Chu, L.-K. Quantifying the Photothermal Efficiency of Gold Nanoparticles using Tryptophan as an in situ Fluorescent Thermometer. *Phys. Chem. Chem. Phys.* **2015**, *17*, 17090−17100.
(54) Kuttner, C.; Holler, R. P. M.; Quintanilla, M.; Schnepf, M. D.; Dulle, M.; Fery, A.; Liz-Marzan, L. M. SERS and Plasmonic Efficiency from Anisotropic Core/Satellite Superstructures. *Nanoscale* **2019**, *11*, 17655−17663.
(55) Leng, C.; Zhang, X.; Xu, F.; Yuan, Y.; Pei, H.; Sun, Z.; Li, L.; Bao, Z. Engineering Gold Nanorod- Copper Sulfide Heterostructures with Enhanced Photothermal Conversion Efficiency and Photostability. *Small* **2018**, *14*, 1703077−1703085.
(56) Baffou, G.; Bordacchini, I.; Baldi, A.; Quidant, R. Simple Experimental Procedures to Distinguish Photothermal from Hot-carrier Processes in Plasmonics. *Light Sci. Appl.* **2020**, *9*, No. 108.
(57) Huang, X.; Kang, B.; Qian, W.; Mackey, M. A.; Chen, P. C.; Oyelere, A. K.; El-Sayed, I. H.; El-Sayed, M. A. Comparative Study of Photothermolysis of Cancer Cells with Nuclear-Targeted or Cytoplasm-Targeted Gold Nanospheres: Continuous Wave or Pulsed Laser. *J. Biomed. Opt.* **2010**, *5*, No. 058002.
(58) Jauffred, L.; Samadi, A.; Klingberg, H.; Bendix, P. M.; Oddershede, L. B. Plasmonic Heating of Nanostructures. *Chem. Rev.* **2019**, *119*, 8087−8130.
(59) Hu, M.; Hartland, G. V. Heat Dissipation for Au Particles in Aqueous Solution: Relaxation Time versus Ssize. *J. Phys. Chem. B* **2002**, *106*, 7029−7033.
(60) Bregnhøj, M.; Rodal-Cedeira, S.; Pastoriza-Santos, I.; Ogilby, P. R. Light Scattering vs. Plasmon Effects: Optical Transitions in Molecular Oxygen Near a Metal Nanoparticle. *J. Phys. Chem. C* **2018**, *122*, 15625−15634.
(61) An, W.; Zhu, Q.; Zhu, T.; Gao, N. Radiative Properties of Gold Nanorod Solutions and its Temperature Distribution under Laser Irradiation: Experimental Investigation. *Exp. Therm. Fluid Sci.* **2013**, *44*, 409−418.
(62) Baffou, G.; Berto, P.; Urena, E. B.; Quidant, R.; Monneret, S.; Polleux, J.; Rigneault, H. Photoinduced Heating of Nanoparticle Arrays. *ACS Nano* **2013**, *7*, 6478−6488.
(63) Moustaoui, H.; Saber, J.; Djeddi, I.; Liu, Q.; Diallo, A. T.; Spadavecchia, J.; Lamy de la Chapelle, M.; Djaker, N. Shape and Size Effect on Photothermal Heat Elevation of Gold Nanoparticles: Absorption Coefficient Experimental Measurement of Spherical and Urchin-shaped Gold Nanoparticles. *J. Phys. Chem. C* **2019**, *123*, 17548−17544.
(64) Jia, H.; Fang, C.; Zhu, X.-M.; Ruan, Q.; Wang, Y.-X.; Wang, J. Synthesis of Absorption Dominant Gold Nanorods and Their Plasmonic Properties. *Langmuir* **2015**, *31*, 7418−7426.

https://doi.org/10.1021/acs.jpcc.1c03898
J. Phys. Chem. C 2021, 125, 16268−16278